Methyl Ferulate Induced Conformational Changes of DeOxyHbS: Implication on Sickle Erythrocyte Polymerization

Ikechukwu Kingsley Ijoma * and **Vincent Ishmael Egbulefu Ajiwe**

Department of Pure and Industrial Chemistry, Nnamdi Azikiwe University, Awka, Nigeria

Abstract: Sickle cell disease (SCD) is a molecular disease caused by substituting glutamic acid with valine at the β-6 position of the hemoglobin, leading to the polymerization of erythrocytes that contain the hemoglobin afterward leads to severe clinical consequences. Polymerization of sickle hemoglobin occurs only in the deoxygenated form i.e only sickle deoxyhemoglobin (DeOxyHbS) polymerizes. SCD is predominant in children living in Africa, especially in West Africa. Therefore, molecular docking and molecular dynamic simulation studies were carried out on methyl ferulate isolated from *Ficus thonningii* leaves, a known antisickling plant used in Eastern Nigeria to manage SCD. The Harborne procedure was used for extraction, whereas the combination of column chromatography and flash chromatography was used for the isolation and purification of active principles of the leaves extract. The structure of methyl ferulate was determined based on nuclear magnetic resonance (NMR) analysis. A binding affinity of -5.8 kcal/mol indicated that methyl ferulate binds to DeOxyHbS and could interfere with the processes that trigger sickle hemoglobin polymerization *in vitro*. The observed variations in perturbation of both DeOxyHbS and FTH3-DeOxyHbS complex root mean square deviation (RMSD), the radius of gyration (R_{gyr}), solvent accessible surface area (SASA), potential energy (PE), and Van der Waal's (VDW) interactions were obtained from the molecular dynamic simulation studies of the binding site amino acid residue performed at 500 ps and suggest that in silico methyl ferulate binds with amino acid residues reported being involved in sickle hemoglobin polymerization and thus may possess antisickling potentials in vitro.

Keywords: Methyl ferulate; computational chemistry; sickle hemoglobin.

1. Introduction

The use of ethnomedicine in treating and managing diseases in the African continent has long been verified. Several studies demonstrated the antisickling properties of various extracts, including *Ficus thonningii* [1]. Sickle cell disease (SCD) is a hereditary genetic disease caused by the mutation of the hemoglobin contained in the erythrocyte. This mutation occurs at β6 position of normal hemoglobin (HbA) i.e., a neutral hydrophobic valine residue is substituted for a negatively charged glutamic acid. Consequently, deoxygenated sickle hemoglobin (DeOxyHbS) molecules aggregate into fibers that form an elongated bundle. This subsequently results in alteration of hemoglobin function and reduction in the flexibility of the erythrocytes [2], which in turn leads to polymerization of DeOxyHbS into 14-stranded helical fibers, which distort/alters the shape of erythrocytes subsequently, this causes several problems associated with vaso-occlusion [2-5]. The mutated Val-β6 has its hydrophobic side chain lodged in a pocket of neighboring sickle hemoglobin (HbS) tetramer, formed by several hydrophobic residues, noteworthy but not exclusive are Ala-β70, Phe-β85, and Leu-β88, as well as the Heme groups [6-8]. SCD is

prominent in West Africa, including Nigeria [9]. Studies suggest that any innocuous agent bound to the region involved in sickling should alter the binding site of sickle deoxyhemoglobin (DeOxyHbS) significantly enough to prevent sickling [10]. Finch *et al.* [11], Josephs *et al.* [12], and Magdoff-Fairchild *et al.* [13] showed that *in vitro,* the sickling fibers are rods composed of four, six, or eight monofilaments helically wound around each other, each monofilament being a string of stacked hemoglobin molecules. This suggests that a single complementary site does not simply cause sickling but that other molecular binding sites play a significant role. Therefore, interfering with any of these contact points of sickle hemoglobin (HbS) might prevent sickling. Also, certain anesthetics and some relatively chemically inert gases have been shown to bind to myoglobin and hemoglobin [10,14].

Since Glu-β6 → Val-β6 mutation occurs at the hemoglobin surface, the structure of DeOxyHbS is not significantly perturbed relative to that of normal deoxygenated hemoglobin (DeOxyHbA) [6-8,15]. Sickle cell hemoglobin (HbS) polymerization is characterized by a delay time [16-18]. It is believed to occur via a double nucleation mechanism, initiated by the formation of HbS fibers (homogeneous

nucleation), followed by fiber growth through nucleation of additional polymers on the surface of existing ones (heterogeneous nucleation) [19,20]. It was proposed that homogenous nucleation proceeds through a two-step mechanism where metastable dense clusters play the role of nucleation precursors [21]. Thus, delaying or preventing the formation of such precursors could signify sickle erythrocyte inhibition.

Protein aggregation is a complex biological process associated with various diseases, including neurodegenerative diseases such as Alzheimer's and Parkinson's diseases and SCD [22,23]. Therefore, understanding the thermodynamics and molecular mechanisms of protein aggregation is critical for developing therapeutic strategies and designing protein aggregation inhibitors. From a molecular perspective, protein aggregation depends on a complex balance of electrostatic and hydrophobic interactions mediated by water and osmolytes [24,25], influencing protein function. For instance, HbS responsible for SCD [2,3,6-8,26-29]. Molecular dynamics has successfully simulated various motions within protein structures [30]. Understanding the magnitudes and time scales of atomic fluctuations in proteins is essential for characterizing the internal motions that play important roles in their biological activity. The interatomic subunit contacts of the four hemoglobin subunits within the hemoglobin tetramer are stabilized by many weak nonbonded interactions [31], which play a vital role in sickle erythrocyte gelation [32]. Therefore, the specific objectives of this research were to evaluate and validate the in silico antisickling potentials of methyl ferulate isolated from *F. thonningii* a known antisickling plant used by the ethnic people of Eastern Nigeria in the management of SCD because the observed bioactivity of plant extracts is attributed to the presence of identified phytochemicals [33-35].

Taxonomy
Ficus thonningii
Kingdom: Plantae
Phylum: Tracheophyta
Class: Magnoliopsida
Order: Rosales
Family: *Moraceae*
Genus: Ficus L.
Species: *Ficus thonningii* Blume [36,37]

Figure 1. *Ficus thonningii* tree with leaves.

2. Experimental

2.1. Preliminary analytical information
The plant leaves collected from the bushes of Nnodo Amike-Aba in Ebonyi Local Government Area, Nigeria, were identified and authenticated as *Ficus thonningii* (Figure 1) at the Department of Applied Biology Ebonyi State University, Abakaliki. All chemicals used for the extractions and purification were sigma Aldrich quality grade (Steinheim, Germany). The melting point was estimated using the Thiele apparatus (Duran, Germany), while samples were weighed using an analytical weighing balance (OHAUS, USA). Both ^{13}C and ^{1}H NMR spectra and *2D* NMR spectra were all recorded using Bruker 500 MHz spectrometer (Bruker, USA). Molecular docking was performed in Autodock tools using vina script, while molecular dynamics simulations were performed using the NAMD program using CHARMM27 all-force field parameter support.

2.2. Method for Extraction, Purification, and Structural Elucidation

Sequential extraction of the plant part was successively carried out separately with solvents of increasing polarity: n-hexane, chloroform, methanol, and methanol-water mixture (4:1). Ten kilograms of the pulverized leaves of *Ficus thonningii* were weighed and soaked in appropriate solvent for about 72 hours resulting in a volume of 2000 mL: 500 mL. The mixture was filtered, and the filtrate was heated in a water bath to one-tenth (1/10) of its initial volume at < 40°C [38]. Each extract was heated to dryness, weighed, and stored in a glass vial at about -4°C. These extracts were thereafter subjected to column chromatography.

2.3. Chromatographic Separation
The column chromatographic technique separated the crude extract of n-hexane, chloroform, methanol, and methanol-Water. The glass column (150 x 1.5 cm. ID) was packed with two-thirds (2/3) of the length with silica gel (70-230 mesh). The glass column was plugged with cotton wool at the bottom, and polytetrafluoroethylene (PTFE) stop cork, 100 mL of chloroform, and methanol mixture (80:5 v/v) were

poured into the column and allowed to drain to the level of the gel bed to condition the system. Then, 15 g of the crude extract was subjected to column chromatography and eluted with hexane-ethyl acetate (80:20, 70:30, 60:40, 50:50), ethyl acetate (100%), and methanol (100%) gradients. The silica gel 70-230 mesh (600 g) slurry was made with the eluting solvent and packed into the glass column. The tap was opened to allow the excess solvent to run off. 15 g of the hexane leaves. Extracts were dissolved in the eluting solvent and packed on the silica gel slurry with a pipette. Immediately on the column setting, glass wool fiber was placed on top of the extract, and the eluting solvent was added. The eluent was collected with 50 mL and 100 mL conical flasks. Further elution was done with increasing concentration gradients. For the methanol leaves crude extracts, elution was carried out using dichloromethane-ethyl acetate (80:20, 70:30), ethyl acetate (100%), ethyl acetate-methanol (50:50), and methanol (100%) gradients. For the fractionation of chloroform leaves crude extract, elution was done with hexane-dichloromethane gradients (60:40, 50:50), ethyl acetate (100%), ethyl acetate-methanol (50:50), and finally with 100% methanol. Elution of methanol-water leaves extract was carried out with dichloromethane-ethyl acetate (80:20), ethyl acetate (100%), and methanol (100%). Compound isolated from the MeOH-Water extract was labeled FTH3. The fraction collected was monitored for purity by spotting on silica gel-coated aluminum thin-layer chromatographic (TLC) plates and viewed under UV light (254 nm). Plates were also placed in iodine chroma tanks to view spots. A spray of 0.5% vanillin and 10% sulphuric acid was used on the plates and the plates were dried in a hot air oven at 110°C for 1 hour and color changes were observed. The pure extracts were subjected to further separation and purification using flash chromatography. Extracts that gave yield of analytical significance after column separation was reported.

2.4. Flash chromatographic separation and Recrystallization

Before NMR analysis, the obtained fraction was purified using flash chromatography (silica gel, mesh 230-400, 30 g). Elution was done with varying proportions of petroleum ether: chloroform (4:1) as the mobile phase. Elution with a solvent mixture of petroleum ether: chloroform (5:1) afforded a single major spot on TLC with some minor impurities at the origin. Concentration, drying, washing, and recrystallization of the fractions severally with methanol afforded FTH3.

2.5. Nuclear Magnetic Resonance (^{1}H-NMR and ^{13}C-NMR)

The Nuclear Magnetic Resonance (NMR) spectral analyses were carried out using a Bruker 500 MHz. Before NMR analysis, the samples were dissolved in DMSO-d6. The spectral determined includes ^{1}H, ^{13}C, DEPT-135, TOCSY, COSY, HSQC and HMBC

2.6. Method for Molecular Docking
2.6.1 Retrieval of Target Protein Structures
Protein Data Bank [39] was used for retrieving the structure of 2HBS [6]. The criteria for selecting the indicated structure were based on PDB advance BLAST analysis. The structure used in this study displayed the maximum score and query cover in BLAST.

2.6.2. Ligand Preparations
The structures of the ligands were drawn, 3D optimization was performed in Chemsketch software, and energy minimization was carried out using Avogadro software. The structures were prepared in Mol2 format and later converted to PDB format using Avogadro. Further shape complementarity principle was applied.

2.6.3. Docking Procedures
The in silico molecular docking analysis was done by the method described by Trott and Olson, 2010 [40]. The docking analysis included retrieval of the structure of the target protein (2HBS) from the PDB database, then drawing of the structures using ChemSketch and energy minimization of the ligands using Avogadro software [41]. Molecular Docking studies were carried out using prepared hemoglobin target macromolecule and isolated compound as a ligand by employing the Autodock Vina program. Docking was performed to obtain a population of possible conformations and orientations for the ligand at the binding site. The protein was loaded in Autodock tool software, creating a PDBQT file that contains a protein structure with hydrogens in all polar residues. All bonds of ligand were set as rotatable. All calculations for protein-fixed ligand-flexible docking were done using the Lamarckian Genetic algorithm (LGA) method. The docking site on the protein target was defined by establishing a grid box with a default grid spacing of 1.000 Å [40]. The grid center was set to 21.5323, 47.0331, and 39.9478 for x, y, and z, respectively, while the box was set to 101.0182x99.5713x71.0608 Å^3 for x, y, and z, respectively. The exhaustiveness was set to a default value of 8. The best conformation with the lowest binding energy was chosen after completing the docking search [40-44]. The interactions of the complex protein-ligand conformations, including hydrogen bonds and the bond lengths, were analyzed using Discovery Studio 3.0 [45] and Pymol [46].

2.7. Method for Molecular Dynamics
The structure of DeOxyHbS (2HbS) reported by Harrington *et al.,* [6] was used in this assay. MD simulations were performed using the NAMD program [47] with CHARMM27 all-force field parameters support and for macromolecules, generalized CHARMM27 all-force field parameters were applied [48,49]. The models were constructed with crystallization water molecules. After that, the resulting models were solvated in a cubic periodic box with water in cubic periodic boundary conditions [50]. Counter ions (Na$^+$, Cl$^-$) neutralized the systems. The distance

between the periodic boundary conditions and the closest protein atom was set to 10.0 Å all through. Before the MD simulation, equilibration and energy minimization were carried out on each system through the steepest descent algorithm with 100,000 steps to avoid steric clashes or improper geometries and to relieve any local stress caused by non-bonded atomic overlaps and bond-length and bond angle distortions under the NVT ensemble. After the minimization, an isothermal-isobaric (NPT) simulation was run by weak coupling to a bath of constant pressure. In our study, the constant temperature control was based on Langevin dynamics [51] with a damping coefficient (gamma) of 1.0 ps. The full-system periodic electrostatics was calculated using the particle-mesh Ewald (PME) algorithm [52-54]. The Molecular Dynamics simulation was carried out for 500 ps for both the protein and protein-ligand complex under normal temperature (310 K) and pressure (1 bar) using a temperature coupling time constant of 0.01 ps and a pressure coupling time constant of 0.02 ps. A distance-dependent dielectric was used to compensate for the absence of explicit solvent.

In the present study, the Velocity-rescaling (modified Berendsen's thermostat) [55] was used for temperature coupling in NVT equilibration, while the Parinello–Rahman barostat [56] was used for pressure coupling during NPT equilibration. Both systems were well equilibrated. The temperature of the systems reached 310 K while the pressure was maintained at 1 bar. The equilibration was followed with a 500 ps long MD production run under NPT ensemble for each system. VDW forces and short-range electrostatic interactions were treated using a cutoff of 10 Å. During the MD run, the LINCS algorithm was used to constrain the lengths of all bonds [57]. Interactions between non-bonded atom pairs were calculated with a smooth cutoff radius of 10 Å. Structures were saved, and the trajectory analysis was carried out on the 500 saved structures. All parameters were estimated from the trajectory analysis. Five hundred structures at intervals of 1 ps each were chosen for further analysis using Visual molecular dynamics (VMD) [58] and Microsoft Excel.

3.   Results and Discussions

3.1. Results of Structural Elucidation
FTH3- Methyl ferulate
Yellowish brown crystal, Rf: 0.83, melting range: 63 - 65 °C [59], mass: 14.68 g yield 0.15%. ^{13}C (500MHZ, DMSO-d6): 167.09 (C-9), 149.36 (C-4), 147.91 (C-3), 145.10 (C-7), 125.55 (C-1), 123.12 (C-6), 115.50 (C-8), 114.19 (C-5), 111.29 (C-2), 55.71 (3-OCH₃), 51.22 (9-OCH₃). ^1H (500MHZ, DMSO-d6): 7.57 (H-7), 7.32 (H-6), 7.12 (H-2), 6.80 (H-5), 6.50 (H-8), 6.46 (4-OH), 3.81 (3-OCH₃), 3.70 (9-OCH₃). The ^{13}C, ^1H, DEPT-135, TOCSY, COSY, HSQC, and HMBC spectra for FTH3 corroborated those of methyl ferulate referenced in the literature and was assigned as Figure 2 [60,61]. Molecular weight 208.21 g/mol.
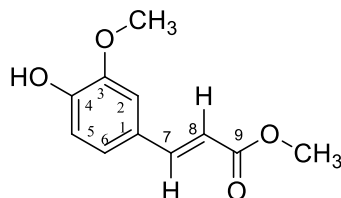

Figure 2. Structure of Methyl ferulate ($C_{11}H_{12}O_4$) isolated from *F. thoninngii* leaves.

3.2. Results of Molecular Docking Assay
From Figure 3, conventional hydrogen bond interaction was made with $LYS_{G:40}$ and $GLU_{G:30}$, Pi-Anion interactions include $ASP_{B:79}$, $HIS_{G:50}$ interaction was Pi-Sigma interaction. At the same time, $LEU_{G:34}$ had a P-Alkyl interaction with FTH3 and VDW interactions which, though may be small, contributed to structural stereochemistry and conformational stability of deoxyhemoglobin as reported by Perutz *et al.* [62]. Lateral contact residues such as $ASP_{B:79}$, and $HIS_{G:50}$ have been implicated in DeOxyHbS polymerization [6] therefore, interactions with these amino acid residues may signify antisickling activity because significant changes in the polymerization properties of HbS occur as a result of altering residues involved in the crystal double-stranded contacts [3].

Residue-Residue salt bridge reported by Galamba and Pipolo [32] for 2HBS includes $1β_1LYS82$ and $2α_2GLU30$, $1β_1ASP79$ and $2β_2LYS120$. In contrast, Residue-Residue repulsion interactions were $1β1ASP79$ and $2α2ASP47$, $1β1ASP79$ and $2β2GLU30$, these salt bridges and repulsion interactions were broken. Its effect is minimized by the interaction of FTH3 with the amino acid residues of $ASP_{C: 79}$ and $GLU_{G: 30}$ (Figure 3), also binding with αlys40 enhances the transition from T⟶R conformation because the interactions between βHis126, αLys40, αArg141, and βVal34 are responsible for the stabilization of the alpha and beta chains and are usually broken during conformational changes in the Deoxy state thus, FTH3 weakens these interactions and decreases the time spent in the Tensed (T) state consequently, these interactions (βHis126, αLys40, αArg141, and βVal34) that once stabilized the deoxygenated form are broken to stabilize the oxygenated form (Relaxed (R) state) of the hemoglobin. Garret and Grisham [63] also reported a similar observation.
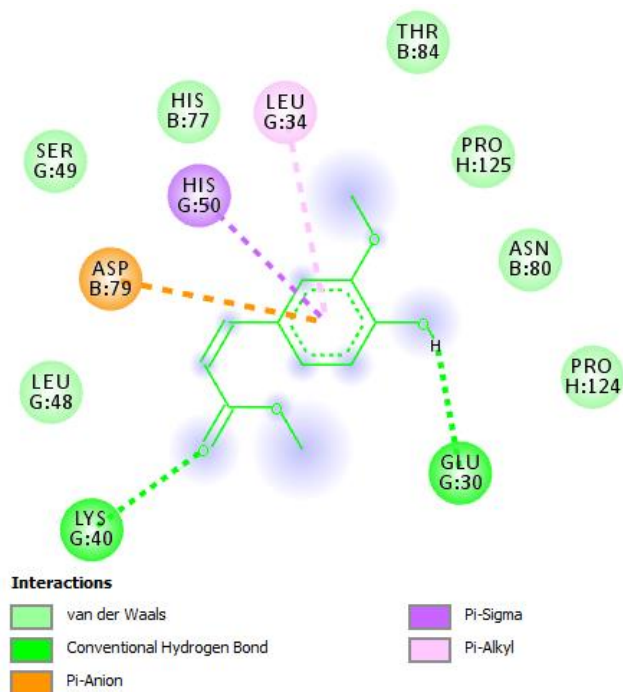
Figure 3. 2D view of FTH3 binding interactions with 2HbS.

Similarly, antisickling molecules may not bind with equal probability to every residue involved in forming salt bridges or strong electrostatic repulsions [32]. The effect of breaking these salt bridges and minimizing residue-residue repulsion is the subsequent inhibition of DeOxyHbS polymerization by FTH3. In addition, the breaking of salt bridges in DeOxyHbS prompts its destabilization, leading to delay and disruption of the polymer formation process. This mechanism favors

T→R transition, which afterward promotes deoxyhemoglobin solubility through stabilizing liganded hemoglobin in the form of R2 and/or the various states of HbS [64]. Moreover, compounds that modify the solubility characteristics of DeOxyHbS prevent the noncovalent bond formation that necessitates polymerization by altering the water structures around DeOxyHbS molecule [65].
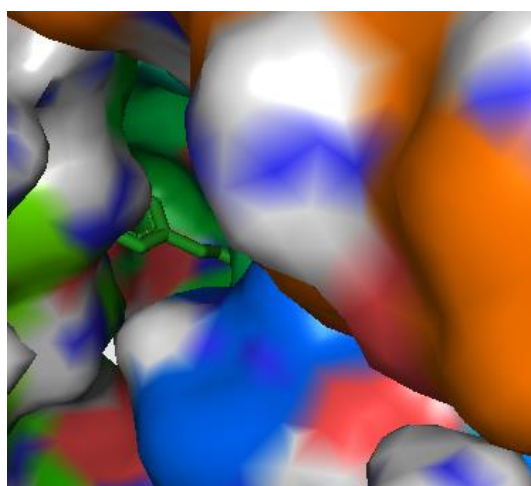

Figure 4. Pose view of FTH3 with 2HbS (binding affinity = -5.8 kcal/mol).

Search for possible antisickling drugs has led to the discovery of a family of compounds that are more powerful allosteric effectors than the natural ones (2, 3-diphosphoglycerate). These allosteric effectors combine with sites far removed from the diphosphoglycerate (DPG) binding site [66]. The results of the molecular docking analysis and interactions of

FTH3 with amino acid residues involved in T → R transition suggest that FTH3 may act as an allosteric effector. Figure 4, shows the pose view of FTH3 in the DeOxyHbS allosteric core. The binding affinity was computed as -5.8 kcal/mol. The binding affinity of FTH3 was -2.8 kcal/mol, lesser than the binding affinity reported by Ross *et al.* [67] and Ross *et al.* [68] for

the deoxyhemoglobin gelation process, which showed that FTH3 could interfere with the processes that trigger sickle erythrocyte polymerization *in vitro*. Research has indicated that the T state structure, when ligated, showed significant changes in the heme

pockets, as well as changes at the α1β2 interface in the direction of the R quaternary structure [69]; hence, FTH3 binding probably favored the R quaternary structure in the direction that favors allosteric properties.
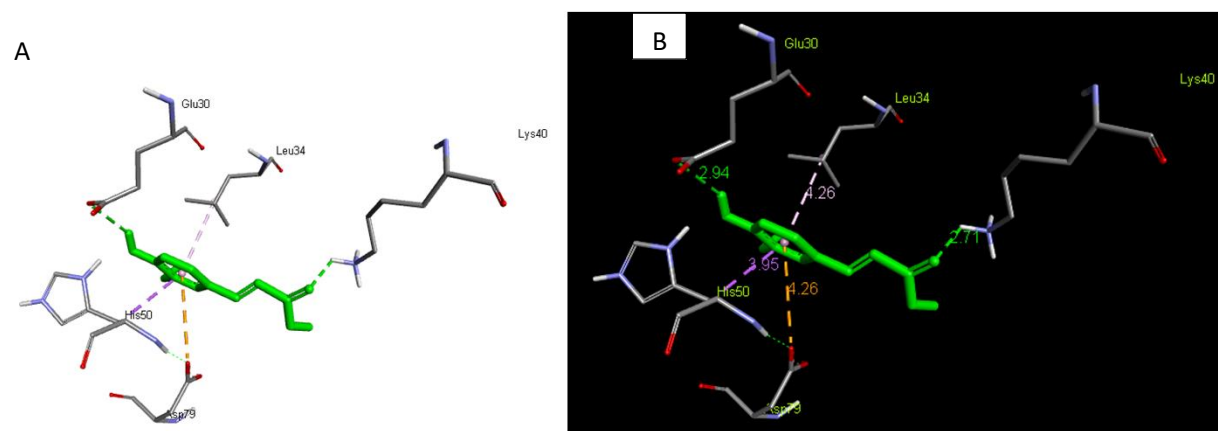

Figure 5. 3D Binding interaction of FTH3 with 2HbS amino acid binding site residue (A) showing distinct bond length (B).

The observed bond interaction of FTH3 to ASP76 was 4.26 Å, HIS50 was 3.95 Å, GLU30 was 2.94 Å, and LEU34 was 4.26 Å whereas LYS40 was 2.71 Å (Figure 5). The presence of a hydrogen bond constraints and stabilizes deoxyhemoglobin; however, ligands can destabilize deoxyhemoglobin by binding

to it [62] subsequently, reducing the time spent in the deoxy state since only DeOxyHbS polymerizes. A hydrogen bond was observed with GLU30 and thus may signify an increase in deoxyhemoglobin's instability, reducing the time spent in the tensed (T) state.
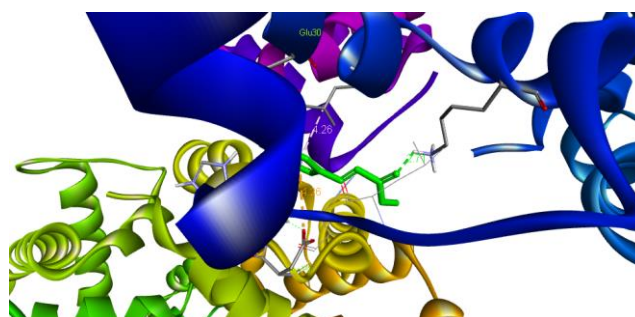

Figure 6. Binding interaction of FTH3 and 2HbS in the presence of surrounding amino acid residues. Bonding and non-bonding interactions act within ≤ 4.26 Å.

Figure 6 showed the interaction of FTH3 in the presence of surrounding amino acid residue exerting maximum VDW interactions at ≤ 4.26 Å. Furthermore, Galamba and Pipolo [32,] using molecular dynamic simulation, have shown that VDW interactions and noncovalent electrostatic interactions are important determinant factors in DeOxyHbS aggregation since they affect the PE at the bound region.

3.3. Results of Molecular Dynamics Simulations
After the simulation run, the estimated RMSD of the crystal structures was 2.541 Å for DeOxyHbS and 2.868 Å for the FTH3-DeOxyHbS complex. The overall folding pattern, the α-helices, and the interatomic subunit associations remained partly

intact throughout the 500 ps simulation trajectory. In our study of DeOxyHbS and FTH3-DeOxyHbS conformations, the substrate FTH3 was docked in DeOxyHbS using the AutoDock tool. The compartment between the docked ligand conformation (gray) and the reference conformation in the crystal structure (black) located in the binding site is shown in Figure 7. The RMSD of the FTH3-DeOxyHbS was 2.868 Å, which differs from the RMSD of the reference (DeOxyHbS). The RMSD analyses of protein backbone atoms and the ligand atomic coordinates were performed to measure the structural stability of the complexes. The RMSD variations of the two systems on 500 ps time scales MD simulation indicated that the complex atomic coordinates and the initial structures are different,

indicating the inability of DeOxyHbS to maintain its structural integrity after FTH3 docking. This may be

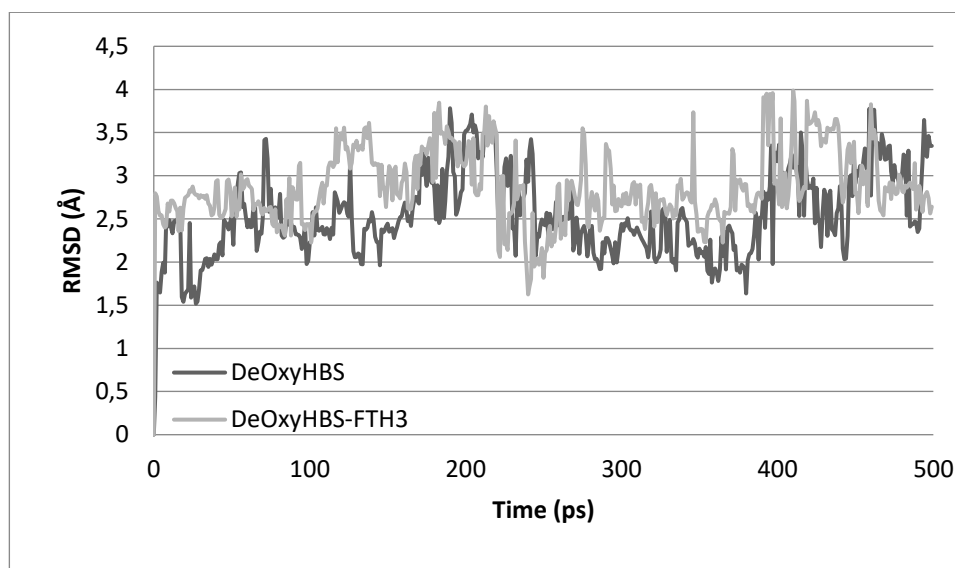because of the short simulation time that didn't permit full-scale energy minimization.

Figure 7. Fluctuations in RMSD of DeOxyHbS model (black) and FTH3-DeOxyHbS complex (gray).
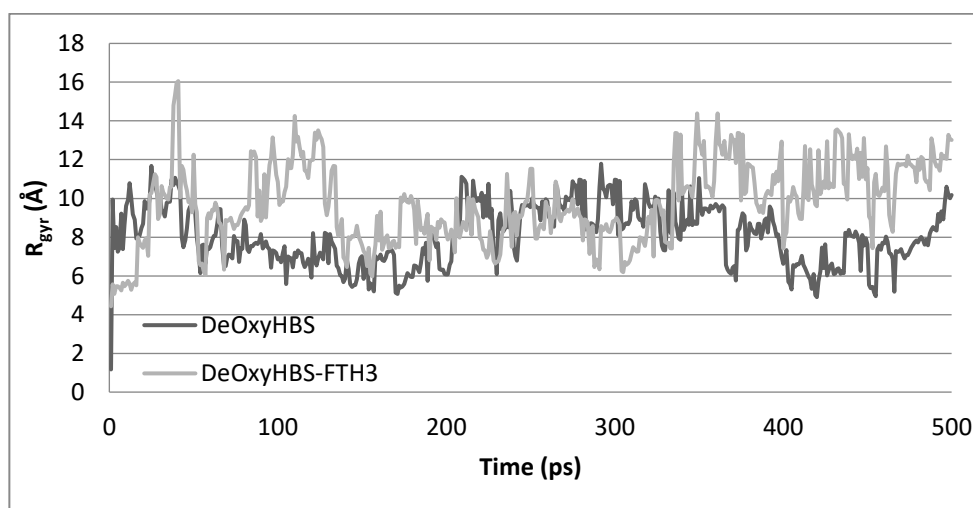

Figure 8. Fluctuations in R_{gyr} of DeOxyHbS (black) and FTH3-DeOxyHbS complex (gray).

The compactness of DeOxyHbS and FTH3-DeOxyHbS is denoted by R_{gyr}, which represents the compactness of the protein structure and is associated with stability [70]. Differences in R_{gyr} values between DeOxyHbS and FTH3-DeOxyHbS are shown in Figure 8. The average R_{gyr} values of DeOxyHbS and FTH3-DeOxyHbS complex were calculated as 8.075 Å, and 9.727 Å, respectively. The FTH3-DeOxyHbS showed an increase in R_{gyr}, suggesting a loss in compactness due to the docking of FTH3.

We also investigated the hydrophobic core region of DeOxyHbS and FTH3-DeOxyHbS by calculating the change in SASA. A significant increment in average SASA has been observed in the FTH3-DeOxyHbS

complex (Figure 9), which showed more substantial changes in the SASA probably because of the interaction of FTH3 with Asp79, His50, Leu34, Lys40, and GLu30 (Figure 3) which renders these residues (Asp79, His50, Leu34, Lys40, and GLu30) more accessible to solvent. Galamba and Pipolo [32] reported Asp79 and GLu30 as Salt bridges in DeOxyHbS, while α Lys40 is among the residues responsible for stabilizing the alpha and beta chains and are usually broken during conformational changes in the Deoxy state [63]. The increase in average SASA suggested that the FTH3-DeOxyHbS complex has a large surface exposed to solvent, which might cause the exposure of hydrophobic residues and contribute partly to FTH3 antisickling potentials.
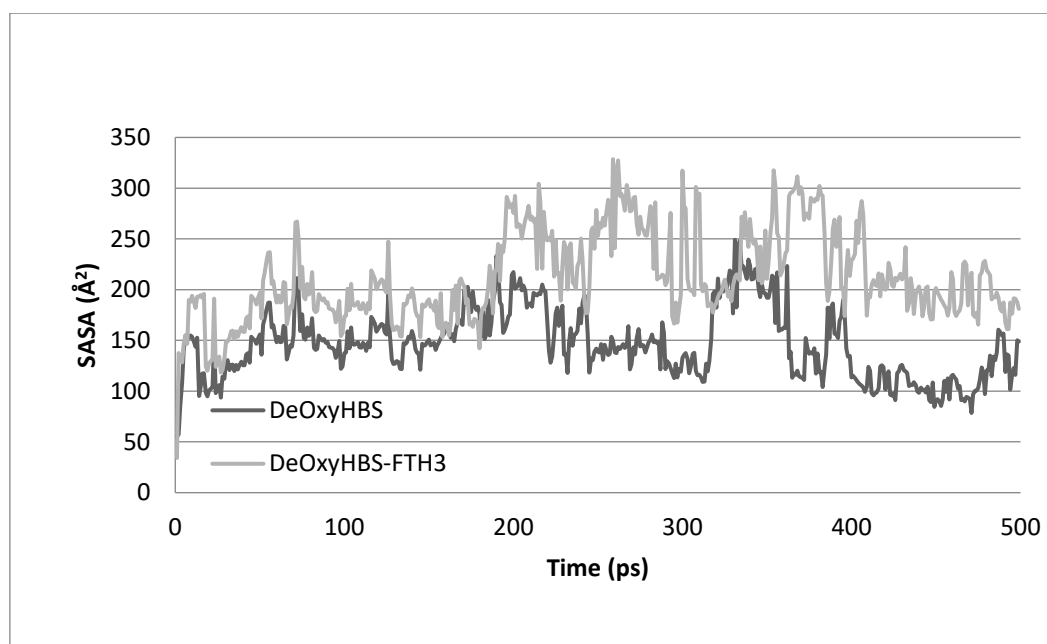
Figure 9. Fluctuations in SASA of DeOxyHbS model (black) and FTH3-DeOxyHbScomplex (gray).

For FTH3-DeOxyHbS, it is interesting to note that although there was a slight increase in the R_{gyr}, the clustering of surface residues led to a slight increase in the surface area necessitated by docking FTH3. The SASA for DeOxyHbS superimposed on FTH3- DeOxyHbS exhibited similar rapid oscillations during the 500 ps of the simulation trajectory. DeOxyHbS contraction in R_{gyr} correlated well with its reduction in solvent-accessible surface area.
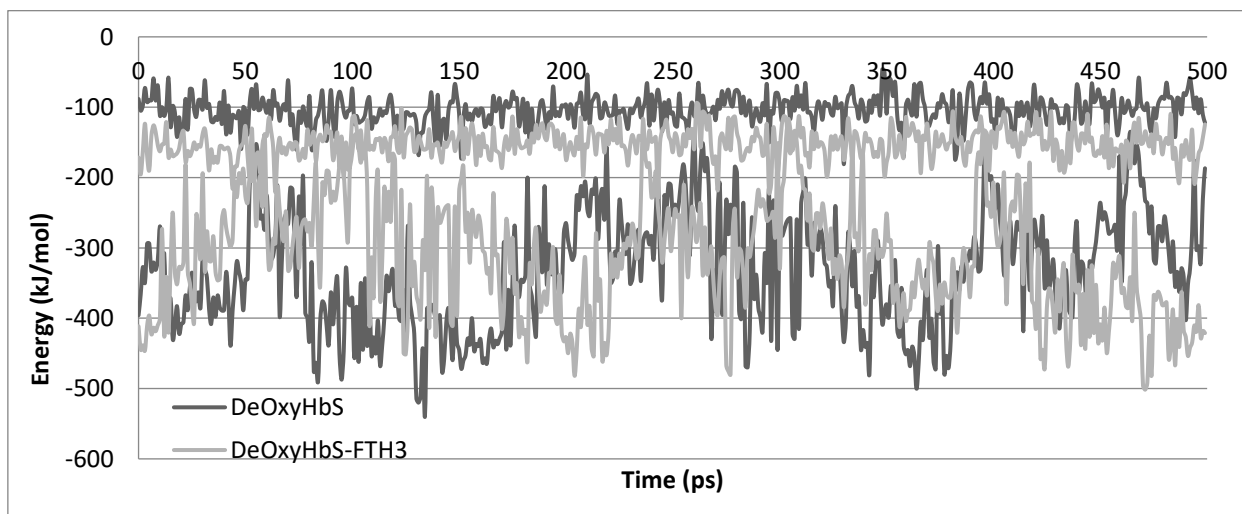

Figure 10. VDW (upper graph) and electrostatic internal energy (lower graph) for FTH3-DeOxyHbS (gray) and DeOxyHbS (black).
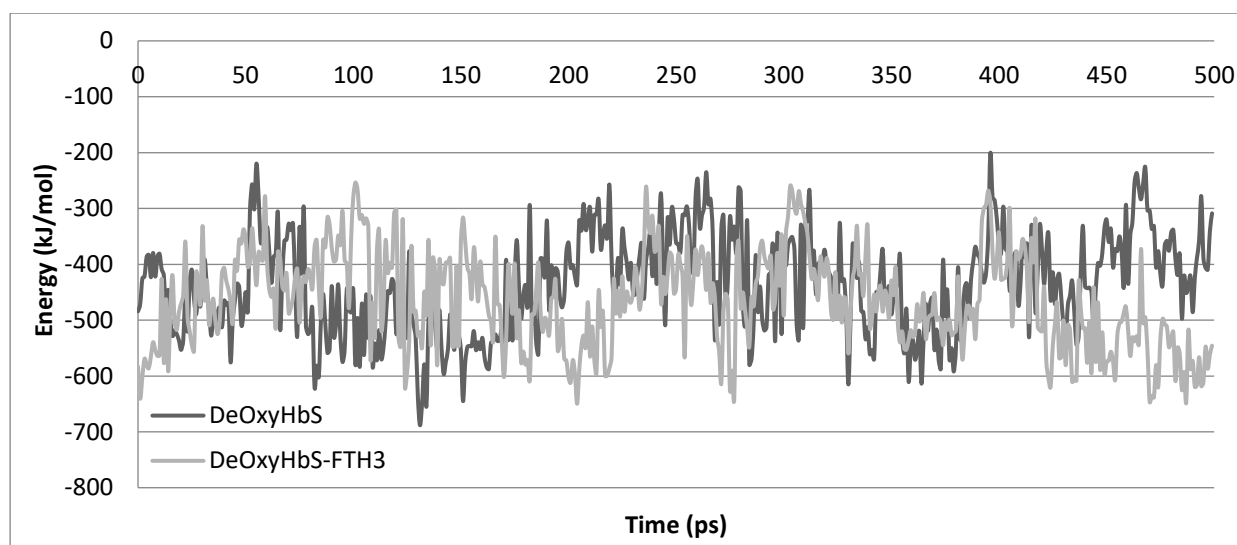
Figure **11.** PE plot of FTH3-DeOxyHbS (gray) and DeOxyHbS (black)

From the observed variation of the simulated trajectory (Figure 10) there was a decrease in VDW energy and an increase in the electrostatic internal energy (EIE) in the bound region for the FTH3-DeOxyHbS simulation in contrast to the DeOxyHbS simulation. Galamba and Pipolo [32] have shown that EIE and VDW energies contribute to the PE along reaction coordinates, showing that both are important in the aggregation process; therefore, although, the interactions due to EIE are much stronger in FTH3-DeOxyHbS when compared to the DeOxyHbS, the sum of all VDW interactions significantly impacted on the PE in the bound region of the FTH3-DeOxyHbS complex (Figure 11). The increase in the EIE indicated that FTH3 could induce salt bridge formation and/or increase the bond energies of the individual atoms involved in bond formation. Still, these interactions were opposed by nonbonded interactions acting at a distance close enough to disrupt these induced effects in the bound region, thus weakening bonds, salt bridge interactions, and residue-residue interactions within the bound region of FTH3 in DeOxyHbS. The calculated mean PE for DeOxyHbS and FTH3-DeOxyHbS within a 500 ps simulation run was -435.725 kJ/mol and -465.492 kJ/mol, respectively, and consequently validated the observed antisickling activity of FTH3 induced by VDW interactions. Our observations showed the impact of VDW interaction on DeOxyHbS polymerization. From the observed simulation trajectory, the calculated mean electrostatic internal energy for FTH3-DeOxyHbS was -325.732 kJ/mol while VDW was -139.76 kJ/mol. Also, the computed average VDW and electrostatic internal energy for DeOxyHbS were -100.97kJ/mol and -334.755 kJ/mol, respectively.

4. Conclusion

The antisickling activity of methyl ferulate isolated from *F. thonningii* leaves was evaluated using a combined in silico approach of molecular docking and molecular dynamics simulation studies. The observed perturbation of the RMSD, R_{gyr}, SASA, EIE, and VDW interactions indicated that methyl ferulate possesses the prerequisite of a potential antisickling agent in silico, thus, in part, validating the use of *F. thonningii* leaves as an antisickling agent in the management of sickle cell patients in Eastern Nigeria. Prospective research on in silico evaluation of methyl ferulate as an antisickling agent should consider extending the simulation time to over 100 ns to fully comprehend the holistic antisickling mechanism of methyl ferulate.. Similarly, other compounds isolated/identified from *F. thonningii* should be considered. Also, to elucidate the various mechanism of extracts of antisickling medicinal herbs, studies on the antisickling potential of compounds in ethnomedicinal therapeutics as it relates to SCD should be considered in silico to fast-track SCD research. Finally, to validate the in-silico assay in vitro, in vivo and clinical trials of methyl ferulate should be considered.

References

1. N.L. Yambeau, P.C. Biapa Nya, C.A Pieme, K.D. Tchouane, C.B. Kengne, Fotsing, P.J. Nya Nkwikeu, A.F. Feudjio, P.B. Telefo, Ethnopharmacological study of the medicinal plants used in the treatment of sickle cell anemia in the west region of Cameroon, *Evid. Based Complement. Altern. Med.,* **2022**, 5098428.
2. W. A. Eaton, J. Hofrichter, S Hemoglobin Gelation and Sickle Cell Disease, *Blood.*, **1987**, 70, 1245–1266.
3. W. A. Eaton, J. Hofrichter, Sickle Cell Hemoglobin Polymerization, *Adv Protein Chem.,* **1990**, 40, 63–79.
4. D.C. Rees, T.N. Williams, M.T. Gladwin, Sickle-Cell Disease, *Lancet.*, **2010**, 376, 2018–2031.
5. R.E. Ware, M. de Montalembert, L. Tshilolo, M.R. Abboud, Sickle Cell Disease, *Lancet.*, **2017**, 390, 311–323.

6. D.J. Harrington, K. Adachi, W.E. Royer, The High-Resolution Crystal Structure of Deoxyhemoglobin S, *J Mol Biol.*, **1997**, 272, 398–407.

7. E.A. Padlan, W.E. Love, Refined Crystal Structure of Deoxyhemoglobin S II. Molecular Interactions in the Crystal, *J Biol Chem.*, **1985**, 260, 8280.

8. E.A. Padlan, W.E. Love, Refined Crystal Structure of Deoxyhemoglobin S I. Restrained Least-Squares Refinement at 3.0-8 Resolution, *J Biol Chem.*, **1985**, 260, 8272.

9. O.E. Nnodu, H.A. Isa, R.I. Chianumba, Y. Tanko, J.H. Iyobosa, J.H. Nnebe-Agumadu, A. Sopekan, C. Ohiaeri, A. Adeniran, G. Shedul, O. Owolabi, A.D. Adekile, O.I. Olopade, F.B. Piel, Implementing newborn screening for sickle cell disease as part of immunization programmes in Nigeria: a feasibility study, *Lancet Haematol.*, **2020**, 7, e534-e540.

10. B.P. Schoenborn, Dichloromethane as an antisickling agent in sickle cell hemoglobin (gas binding to hemoglobin/sickle cell disease), *Proc Natl Acad Sci.,* **1976**, 73, 4195-4199.

11. J.T. Finch, M.F. Perutz, J.F. Bertles, J. Dobler, Structure of sickle etythrocyte and of sickle-cell hemoglobin fibers, *Proc Natl Acad of Science, USA.*, **1973**, 70, 718-722.

12. R. Josephs, H.S. Jarosch, S.J. Edelstein, Polymorphism of sickle cell hemoglobin fibers, *J Mol Biol.*, **1976**, 102, 409-426.

13. B. Magdoff-Fairchild, P.H. Swerdlow, J.F. Bertles, Intermolecular organization of deoxygenated sickle hemoglobin determined by x-ray diffraction, *Nature*, **1972**, 239, 217-219.

14. B.P. Schoenborn, Binding of Xenon to Horse Haemoglobin, *Nature*, **1965**, 208, 760-762.

15. M.F. Perutz, G. Fermi, D.J. Abraham, C. Poyart, E. Bursaux, Hemoglobin as a Receptor of Drugs and Peptides: X-Ray Studies of the Stereochemistry of Binding, *J Amer Chem Soc.,* **1986**, 108, 1064–1078.

16. K. Adachi, T. Asakura, Demonstration of a Delay Time during Aggregation of Diluted Solutions of Deoxyhemoglobin S and Hemoglobin CHarlem in Concentrated Phosphate Buffer, *J Biol Chem.*, **1978**, 253, 6641–6643.

17. K. Adachi, T. Asakura, Nucleation-Controlled Aggregation of Deoxyhemoglobin S. Possible Difference in the Size of Nuclei in Different Phosphate Concentrations, *J Biol Chem.*, **1979**, 254, 7765–7771.

18. K. Adachi, T. Asakura, Kinetics of the Polymerization of Hemoglobin in High and Low Phosphate Buffers. *Blood Cell*s., **1982**, 8, 213–224.

19. F.A. Ferrone, J. Hofrichter, W.A. Eaton, Kinetics of Sickle Hemoglobin Polymerization. I. Studies Using Temperature-Jump and Laser Photolysis Techniques, *J Mol Biol.*, **1985**, 183, 591–610.

20. F.A. Ferrone, J. Hofrichter, W.A. Eaton, Kinetics of Sickle Hemoglobin Polymerization. II. A Double Nucleation Mechanism, *J Mol Biol.*, **1985**, 183, 611–631.

21. O. Galkin, W. Pan, L. Filobelo, R.E. Hirsch, R. Nagel, P.G. Vekilov, Two-Step Mechanism of Homogeneous Nucleation of Sickle Cell Hemoglobin Polymers, *Biophys J.*, **2017**, 93, 902–913.

22. A. Horwich, Protein Aggregation in Disease: A Role for Folding Intermediates Forming Specific Multimeric Interactions, *J Clin Invest.,* **2002**, 110, 1221–1232.

23. C.A. Ross, M.A. Poirier, Protein aggregation and neurodegenerative disease, *Nat Med.*, **2004**, 10, S10–S17.

24. P. Ball, Water Is an Active Matrix of Life for Cell and Molecular Biology, *Proc Natl Acad Sci, USA.*, **2017**, 201703781.

25. M.C. Bellissent-Funel, A. Hassanali, M. Havenith, R. Henchman, P. Pohl, F. Sterpone, D. van der Spoel, Y. Xu, A.E. Garcia, Water Determines the Structure and Dynamics of Proteins, *Chem Rev.*, **2016**, 116, 7673–7697.

26. V.M.A. Ingram, Specific Chemical Difference Between the Globins of Normal Human and Sickle-Cell Anamia Hamoglobin, *Nature*, **1956**, 178, 792–794.

27. M. Murayama, Molecular Mechanism of Red Cell "Sickling.", *Science*, **1966**, 153, 145–149.

28. C.T. Noguchi, A.N. Schechter, Sickle Hemoglobin Polymerization in Solution and Cells, *Annu Rev Biophys Biophys Chem.*, **1985**, 14, 239–263.

29. L.L. Pauling, H.A. Itano, S.J. Singer, I.C. Wells, Sickle Cell Anemia, a Molecular Disease. *Science*, **1949**, 110, 543.

30. J.A. McCammon, S.C. Harvey, Dynamics of Proteins and Nucleic Acids, Cambridge University Press, Cambridge, **1987**, 260, 8272-8279.

31. H. Muirhead, J.M. Cox, L. Mazzarella, M.F. Perutz, Structure and function of hemoglobin: III. A Three-dimensional Fourier synthesis of human deoxyhemoglobin at 5.5 Å resolution, *J Mol Biol.*, **1976**, 28, 117-156.

32. N. Galamba, S. Pipolo, On the Binding Free Energy and Molecular Origin of Sickle Cell Hemoglobin Aggregation, *J Phys Chem.,* **2018**, 2-30.

33. K.I. Ijoma, V.I.E. Ajiwe, C.O. Alisa, Antimicrobial Analysis and Structural Elucidation of Active Compounds of *Nauclea latifolia* Stem Extract (Pin Cushion Tree), *Amer J Chem Appl.*, **2017**, 4, 21-26.

34. K.I. Ijoma, V.I.E. Ajiwe, C.I. Awuzie, Antimicrobial Analysis and Structural Elucidation of Active Compounds of *Dialium indum* leaves extract (Velvet Tarmarind), *Int J Pharm Chem.*, **2016**, 6, 237-244.

35. K.I. Ijoma, V.I.E. Ajiwe, Phytochemical Screening of *Dialium indum* leaf extract (Velvet Tarmarind), *Int J Phytopharm.*, **2017**, 7, 6-13.

36. Y. Roskov, G. Ower, T. Orrell, D. Nicolson,

N. Bailly, P.M. Kirk, T. Bourgoin, R.E. Dewalt, W. Decock, E. Nieukerken, L. Penev, Specie 2000, *Naturalis, Leiden, the Netherland*, **2020**.

37. Global Biodiversity Information Facility Secretariat. *Ficus thonningii* Blume. GBIF Backbone Taxonomy, *Checklist dataset*, **2019**.

38. J.B. Harbone, Phytochemical Methods- A guide to modern techniques of plant analysis, 3rd edition, London, Chapman and Hall, **1998**, 6-7.

39. F.C. Bernstein, T.F. Koetzle, G.J. Williams, E.F. Meyer, M.A. Jr., M.D. Brice, J.R. Rodgers, O. Kennard, T. Shimanouchi, M. Tasumi, The protein data bank: a computer-based archival file for macromolecular structures. *J Mol Biol.*, **1977**, 25, 535-542.

40. O. Trott, A.J. Olson, AutoDock Vina: improving the speed and accuracy of docking with a new scoring function, efficient optimization and multithreading, *J Comput Chem.*, **2010**, 31, 455-461.

41. M.D. Hanwell, D.E. Curtis, D.C. Lonie, T. Vandermeersch, E. Zurek, G.R. Hutchison, Avogadro: An advanced semantic chemical editor, visualization, and analysis platform, *J Cheminform.*, **2012**, 4, 17

42. L. Ferreira, R. dos Santos, G. Oliva, A.D. Andricopulo, Molecular docking and structure-based drug design strategies, *Molecules*, **2015**, 20, 13384–13421.

43. D.S. Godsell, G.M. Morris, A.J. Olson, Automated docking of flexible ligands: Applications of AutoDock, *J Mol Recogn.*, **1996**, 9, 1–5.

44. G.M. Morris, R. Huey, A.J. Olson, Using autodock for ligand-receptor docking, *Curr Protoc Bioinform.*, **2008**, 24, 8–14.

45. Biovia Dassault Systemes. Discovery studio visualizer **2020**. San Diego, CA, USA.

46. W.L. Delano, Pymol: An open-source molecular graphics tool. *CCP 4 Newsletter on Protein crystallography*, **2002**, 40, 82-92.

47. J.C. Philips, R. Braun, W. Wang, J. Gumbart, E. Tajkhorshid, E. Villa, C. Chipot, C.R.D. Skeel, L. Kale, K. Schulten, Scalable molecular dynamics with NAMD, *J Comput Chem.*, **2005**, 26, 1781-1802.

48. R.B. Best, X. Zhu, J. Shim, E.M. Lopes, J. Mittal, M. Feig, A.D. Mackerell, Jr, Optimization of the Additive CHARMM All-Atom Protein Force Field Targeting Improved Sampling of the Backbone φ, ψ and Side-Chain χ1 and χ2 Dihedral Angles, *J Chem Theory Comput.*, **2012**, 8, 3257–3273.

49. M.A. Jr, M. Feig, B.C. Rd, Extending the treatment of backbone energetics in protein force fields: limitations of gas-phase quantum mechanics in reproducing protein conformational distributions in molecular dynamics simulations, *J Comput Chem.,* **2004**, 25, 1400–1415.

50. M.F. Harrach, B. Drossel, Structure and dynamics of TIP3P, TIP4P, and TIP5P water near smooth and atomistic walls of different hydroaffinity, *J Chem Phys*., **2014**, 140, 3393–3393.

51. T. Schlick, Molecular Modeling and Simulation, *Springer*, **2002**, 1-162.

52. D.S. Cerutti, R.E. Duke, T.A. Darden, T. P. Lybrand, Staggered Mesh Ewald: an extension of the smooth particle-mesh Ewald method adding great versatility, *J Chem Theory Comput.*, **2009**, 5, 2322.

53. T. Darden, D. York, L. Pedersen, Particle mesh Ewald: An Nšlog (N) method for Ewald sums in large systems. *J Chem Phys*, **1993**, 98, 10089–10092.

54. U. Essmann, L. Perera, M.L. Berkowitz, T. Darden, H. Lee, G.L. Pedersen, A smooth particle mesh Ewald method, *J Chem Phys.*, **1995**, 103, 8577–93.

55. G. Bussi, D. Donadio, M. Parrinello, Canonical sampling through velocity rescaling, *J Chem Phys.*, **2007**, 126, 014101.

56. M. Parrinello, A. Rahman, Polymorphic transitions in single crystals: a new molecular dynamics method, *J Appl Phys.*, **1981**, 52, 7182–90.

57. B. Hess, H. Bekker, H.J.C. Berendsen, J.G.E.M. Fraaije, LINCS: A Linear Constraint Solver for molecular simulations, *J Comput Chem.*, **1997**, 18, 1463–72.

58. W. Humphrey, A. Dalke, K. Schulten, VMD: visual molecular dynamics, *J Mol Graph.*, **1996**, 14, 33–38.

59. A. Tanaka, A. Kato, T. Tsuchiya, Isolation of Methyl ferulate From Rice Bran Oil, *J Amer Oil Chem Soc.*, **1971**, 48, 95-97.

60. A. Ilmiawati, D. Anggraini, G. Syahbirin, D.U. Rahayu, D. U. P. Sugita, Methyl Ferulate from Methanol Extract of Indonesian Sausage Fruit (Kigelia Africana). The 8th International Conference of the Indonesian Chemical Society (ICICS), *AIP Conference Proceedings*, **2000**, 2243, 030009-1–030009-5.

61. N.T.M., Phuong, T.T. Cuong, D.N. Quang, Anti-inflammatory activity of Methyl Ferulate isolated from *Stemona tuberosa* Lour, *Asian Pac J Trop Med.,* **2014**, 7(Suppl 1), S327-S331.

62. M.F. Perutz, Mechanisms regulating the reactions of human hemoglobin with oxygen and carbon monoxide *Annu Rev Physiol.*, **1990**, 52, 1-25.

63. R.H. Garrett, C.M. Grisham, Biochemistry, 4th edition, Cengage learning, **2013**.

64. M.K. Safo, O. Abdulmalik, R. Danso-Danquah, J.C. Burnett, S. Nokuri, G.S. Joshi, F.N., Musayev, T. Asakura, D.J. Abraham, Structural basis for the potent antisickling effect of a novel class of five-membered heterocyclic aldehydic compounds, *J Med Chem.*, **2004**, 47, 4665–4676.

65. M.R. Waterman, K. Yamaoka, L. Dahm, J. Taylor, G.L. Cottam, Noncovalent modification of deoxyhemoglobin S and erythrocyte sickling. Proc Natl Acad Sci USA, **1974**, 71, 2222-2226.

66. M.F. Perutz, Stereochemistry of Cooperative Effects in Haemoglobin: Haem–Haem Interaction

and the Problem of Allostery, *Nature.*, **1970**, 228, 726–734.

67. P.D. Ross, J. Hofrichter, W.A. Eaton, Calorimetric and optical characterization of sickle cell hemoglobin. *J Mol Biol.*, **1975**, 96, 239-256.

68. P.D. Ross, J. Hofrichter, W.A. Eaton, Thermodynamics of gelation of sickle cell hemoglobin, *J Mol Biol.*, **1977**, 115, 111-134.

69. M.K. Safo, M.H. Ahmed, M.S. Ghatge, T. Boyiri, Hemoglobin-Ligand binding: Understanding Hb Function and Allostery on atomic level, *Biochim Biophys Acta.,* **2011***,* 1814, 797–809.

70. M.Y. Lobanov, N. Bogatyreva, O. Galzitskaya, Radius of gyration as an indicator of protein structure compactness, *Mol Biol (Mosk).*, **2008**, 42, 623–628.

NOTES

1. Biovia Discovery studio homepage can be accessed at https://discover.3ds.com/discovery-studio-visualizer-download
2. Information on NAMD program can be found at www.ks.uiuc.edu/Research/namd/
3. Avogadro homepage www.avogadro.cc
4. Information on Autodock tools and vina script can be accessed using www.autodock.scripps.edu
5. VMD home page www.ks.uiuc.edu/Research/vmd
6. Chemsketch homepage www.acdlabs.com/resources/freeware/chemsketch/index.php
7. More information on CHARMM GUI can be found at www.charmm-gui.org
8. Information on the PDB file format can be found at www.rcsb.org/structure/2HBS
9. Microsoft windows environment and Excel can be found at www.microsoft.com